minerals

MDPI

Article

Mechanical Properties and Hydration Mechanism of Coal Flotation Tailing Cemented Filling Materials

Dehao Li [1,2], Yuping Fan [1,*], Xianshu Dong [1,2,*], Xiaomin Ma [1] and Pei Liu [1]

[1] Department of Mining Engineering, Taiyuan University of Technology, Taiyuan 030024, China
[2] Shanxi Ecological Mining Engineering Research Centre, Taiyuan 030024, China
* Correspondence: fanyuping@tyut.edu.cn (Y.F.); dongxianshu@tyut.edu.cn (X.D.)

Abstract: Large-scale application of filled coal mining technology has long been limited by conditions such as the cost of filling. Compared to traditional filling materials, coal flotation tailing filling materials (CFTFM) offers advantages such as low cost and excellent performance. The Box–Behnken response surface method was used to investigate the influence of flotation tailing properties on the mechanical properties and hydration mechanisms of the filling material. Ash content, blending, and calcination temperature of the flotation tailings were used as the investigating factors, and uniaxial compressive strength (7d and 28d), slump, and the slurry water secretion rate of the filling material as the evaluation indicators. The results showed that the influence of the flotation tailings on the uniaxial compressive strength (28d) of CFTFM followed the order ash > calcination temperature > doping, with the interaction of ash and calcination temperature having a greater influence on the uniaxial compressive strength. The optimized pre-treatment conditions for the flotation tailings were 59% ash, 30% doping, a calcination temperature of 765 °C, and optimum uniaxial compressive strength of 7.02 MPa. The effect of flotation tailings on the exotherm of CFTFM hydration was determined using a TAM Air isothermal microcalorimeter, mainly in the induction and acceleration phases. Combined with SEM electron microscopy and IR FT-IR analysis of the hydration products, a descriptive model of the CFTFM hydration mechanism was established. CFTFM hydration can be described in three phases: diffusion, hydration, and hardening. The CFTFM prepared in this study is applicable to the integrated mining and charging synergistic mining technology, which can effectively reduce gangue lifting energy consumption and washing process waste, reduce the cost of filling, and can effectively achieve harmless, resourceful, and large-scale disposal of coal-based solid waste.

Keywords: coal flotation tailings; coal-based solid waste; cemented paste backfills; response surface methodology

Citation: Li, D.; Fan, Y.; Dong, X.; Ma, X.; Liu, P. Mechanical Properties and Hydration Mechanism of Coal Flotation Tailing Cemented Filling Materials. *Minerals* **2023**, *13*, 389. https://doi.org/10.3390/min13030389

Academic Editors: Abbas Taheri, Yanli Huang and Junmeng Li

Received: 17 January 2023
Revised: 19 February 2023
Accepted: 8 March 2023
Published: 10 March 2023

1. Introduction

Ground subsidence, environmental damage, and other problems in coal mining processes exist in large numbers [1], and coal mining subsidence area management has attracted substantial attention from all sectors of society. Filled mining technology covers fields such as mine safety production, ecological environment management, and comprehensive utilization of solid waste, which is an effective way to realize green mining [2]. The single source of traditional filling materials, and the low utilization rate of solid waste are some of the main factors limiting the large-scale application of filling and mining technology. The development of new filling materials with high efficiency, high quality, low cost, and environmental friendliness has gained attention in current research. The coal flotation tailings originate from the fine-grained tailings left after the sorting of raw coal in the coal production process, with kaolin being the main component. It contains a large amount of active Si, Al, and other volcanic ash materials that can react with cement to promote the hydration process of the filling material and improve the early strength. It

can replace part of the cement in the preparation of the filling material, which can not only solve the problem of insufficient filling materials, but also effectively reduce the filling cost.

Currently, the commonly used filling materials in coal mine infill mining are waste rock cemented filling materials, full tailings, cemented sand filling materials, cemented red mud filling materials, and paste-pumped filling materials [3]. Guorui et al. [4] investigated the effect of fine and coarse concrete aggregates on the performance of filler materials using waste concrete as aggregates. Conventional filler materials are made from a single source, which is expensive and inefficient. Coal flotation tailings exhibit good volcanic ash activity, and can be blended with cement to produce cost-effective cementitious materials. The volcanic ash activity of flotation tailings can be determined by direct and indirect methods, including acid-base dissolution, the Frattini test, the saturated lime method, and thermal analysis. The indirect method is primarily a compressive strength test [5]. As a waste product of the coal washing process, coal flotation tailings currently have few integrated use pathways and undergo substantial wastage. Flotation tailings can be activated using certain methods to significantly increase volcanic ash activity. Current methods for the activation of tailings include physical activation [6], chemical activation [7], thermal activation [8], and microwave irradiation activation [9]. The preparation of filling materials from activated coal flotation tailings and coal-based solid waste, such as coal gangue, can significantly reduce filling costs and improve the efficiency of solid waste utilization. The performance requirements of the filling materials vary with application. Commonly used performance indicators for filling materials in coal filling and mining are the uniaxial compressive strength (7d, 28d) and slump, which characterize the mechanical properties of the filling material [10] and rheological properties of the transport process [11], respectively. Hou et al. [12] conducted rheological tests on tailing slurries with different slurry concentrations, and concluded that both the yield stress and plastic viscosity tended to increase with increasing slurry concentrations. To further investigate the factors influencing the performance of the filling material and its mechanism of action, it is necessary to study the hydration process of the filling material and the formation of hydration products from a microscopic perspective. The most common method for studying the hydration process is to test the exothermic rate curve of hydration, which is the kinetic characteristic of the hydration of the reaction sample. By measuring the exothermic rate of hydration of fly ash paste-filled materials, Bo et al. [13] analyzed the characteristics of the changes in each stage of the hydration kinetic process, and revealed the general rules of the structure of the filling material and its formation process. Many scholars have proposed hydration kinetic models based on the hydration law of silicate cement [14,15], laying the foundation for subsequent research on the hydration mechanism of solid waste cementitious materials. Previous research has focused on examining material ratios of filling materials, and there is a lack of understanding of the influence mechanism of performance indicators. Building a relationship between the performance of the filling material and the influencing factors, and finding the best material ratio for the filling material, are key directions for research on the efficient use of coal-based solid waste materials to prepare coal mine filling materials with excellent performance and at low cost. Therefore, this study analyzes the nature of coal tailings and mixes it with other coal-based solid waste, to prepare filling materials in order to improve the efficiency of solid waste utilization and reduce the cost of filling mining.

This study investigated the effects of ash content, proportions, and calcination temperature of flotation tailings on the uniaxial compressive strength (7d and 28d), slump, and secretion rate of the coal flotation tailing filling materials (CFTFM). Response surface analysis was used to conduct an experimental study on the optimum pre-treatment conditions for flotation tailings in filling materials. The relationship between pre-treatment conditions for flotation tailings and the performance of the CFTFM was constructed to determine the optimum pre-treatment conditions for flotation tailings. The exothermic characteristics of the CFTFM hydration were determined using the heat of hydration method, and combined

with the analysis of hydration products to develop a descriptive model of the hydration mechanism of flotation the CFTFM.

2. Materials

The CFTFM consists of two parts: aggregate and cementing materials. The gangue was extracted from the coal processing plant in Xiqu, Gujiao, Shanxi Province, and after crushing and screening, was divided into three grades: <5 mm, 5–10 mm, and 10–15 mm. The three grades of gangue were mixed in a 4:3:3 ratio as filler aggregates. The cementitious material was prepared by mixing cement and flotation tailings in a certain proportion, of which Lionhead ordinary silicate cement was used with a standard of 42.5 R. The main components included SiO_2, Al_2O_3, Fe_2O_3, CaO, MgO, etc. The content of each substance is shown in Table 1.

Table 1. Oxide content in raw materials (%).

Oxide	Coal Flotation Tailings	Cement
SiO_2	53.88	22.36
Al_2O_3	33.58	6.53
Fe_2O_3	4.74	3.36
CaO	1.9	61.48
MgO	0.53	1.17
K_2O	1.762	1.82
SO_3	1.03	1.76
Na_2O	0.238	0.30
P_2O_5	0.166	0.14
MnO	0.035	0.55
ZnO	0.048	0.056
SrO	0.042	0.046
ZrO_2	0.054	0.048
Cr_2O_3	0.029	0.022
BaO	0.026	0.027
CuO	0.023	0.026
PbO	0.017	0.012
LOI	10.8	1.94

The XRD profiles of the main raw materials are shown in Figure 1. The tailings mainly consisted of kaolinite, quartz, mullite, and crystalline aluminum silicate. The graph shows a scattering peak at 20–25°, indicating that the tail coal contains some undecomposed carbon material. The silica and aluminum elements in flotation tailings and gangue exist in large quantities in different forms, providing a rich source of silica and aluminum for the cementation system. The main physical phases of the cement are quartz, mullite, and crystalline aluminum silicate. The chemical compositions of the flotation tailings and cement were determined using XRF. The flotation tailings were extracted from the Gujiao mine and consisted mainly of SiO_2 (53.88%), Al_2O_3 (33.58%), Fe_2O_3 (4.74%), CaO (1.9%), MgO (0.53%), and organic matter.

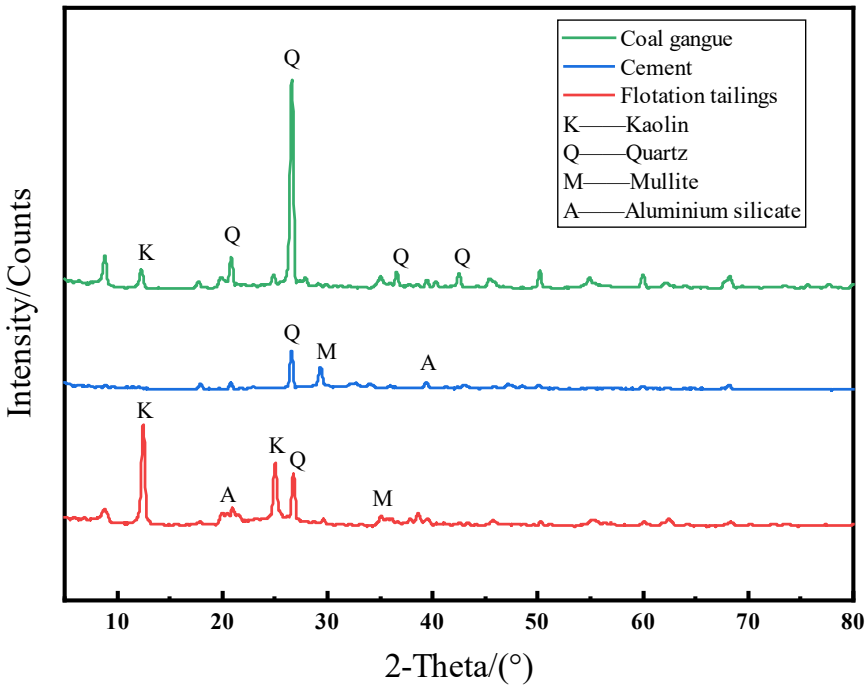

Figure 1. X-ray diffraction pattern of the raw material.

3. Experiments

3.1. Material Proportioning

The filling material was prepared by mixing gangue, cement, and flotation tailings in a 1:5 ratio of cement to sand. The aggregates are divided into three particle sizes: <5 mm, 5–10 mm, and 10–15 mm, accounting for 40%, 31%, and 29% respectively. After mixing, the slurry was mixed with water to a mass concentration of 78%.

3.2. Test Methods and Technical Route

In the single-factor test, each group of specimens were weighed according to the test protocol, mixed with water, and homogenized in a mixer to form filling slurry. A portion of the filling slurry was used for determining the slump and water secretions, while the remaining filling slurry was poured into 100 mm × 100 mm × 100 mm molds to prepare test blocks for compressive strength testing (7d and 28d). Figure 2 shows a technical roadmap for performance testing of the CFTFM.

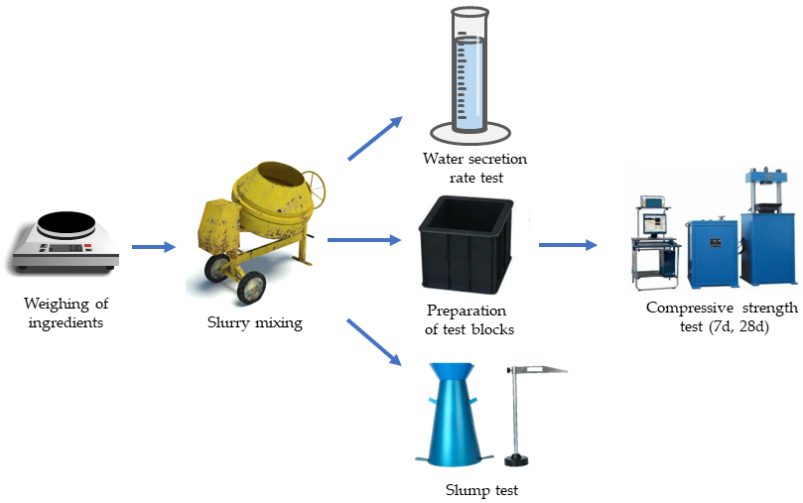

Figure 2. CFTFM performance testing technology roadmap.

The specimen preparation and performance indices were determined by the national standards "GB/T50080-2016 standard test method for the performance of ordinary concrete mixes" [16], "GB/T1346-2011 cement standard consistency water consumption, setting time stability test method" [17], "GB/T50081-2019 Standard for test methods of concrete physical and mechanical properties" [18] and "GB/T23561.10-2010 Methods for Determination of Physical and Mechanical Properties of Coal and Rock" [19] and other standard specifications.

3.3. Single-Factor Test for Optimization of Flotation Tailings Pre-Treatment Conditions

The effects of ash content, proportion, and calcination temperature of the flotation tailings on the uniaxial compressive strength (7d, 28d), slump, and water secretion rate of the CFTFM were investigated separately.

3.4. Response Surface Testing

Based on the single-factor test, the ash (A), proportions (B), and calcination temperature (C) of the flotation tailings were selected as the investigation factors, the uniaxial compressive strength (Y) of the CFTFM was used as the response value, and a 3-factor, 3-level experimental design was carried out using Design-Expert software. The factors and levels of the response surface tests are presented in Table 2.

Table 2. Response surface test factors and levels.

Level	Factors		
	A. Ash/%	**B. Proportions/(*w*t%)**	**C. Calcination Temperature/°C**
−1	50.1	10	650
0	60.55	30	800
1	71	50	950

3.5. Exothermic Hydration Test

Currently, there are two main standards for measuring the heat of hydration: direct and indirect. A TAM Air 8-channel Isothermal Calorimeter was used to test the exothermic properties of the CFTFM hydration. Compared to the traditional heat of dissolution method, isothermal calorimetry is a more accurate and reliable, non-destructive testing technique with continuous tracking of changes in the heat of the hydration of materials.

Test procedure:

(1) Sample pre-treatment, grinding the solid sample to the same fineness as the cement, drying it in an oven at 75 °C for 30 min before testing, and cooling to room temperature.
(2) According to the scheme presented in Table 3, the masses of the specimens were weighed separately using an analytical balance with an accuracy of 0.0001 g, and 300 μL of deionized water was measured using a pipette.
(3) The room temperature was set at 20 °C and the test sample was left at a constant temperature for 2 h or more. The instrument was switched on to ensure that the temperature of all channels of the microcalorimeter was stable.
(4) The raw material was loaded into the corresponding numbered ampoule, stirred quickly with water, and sealed quickly with a cap into the TAM Air 8-channel isothermal microcalorimetry cell. The corresponding reference sample was placed into the reference cell at the same time.
(5) The resulting heat flow lines were exported and processed for analysis using data processing software.

According to the response surface optimization test, the tailing coal pre-treatment conditions were determined to be 59% ash, 30% proportion, and a calcination temperature of 765 °C. A new cementitious material was prepared as a mineral admixture mixed with cement. The heats of hydration of pure cement specimen S1 and proportionally optimized

specimen S2 were tested separately. The heat of the hydration test protocol is presented in Table 3.

Table 3. Specimen hydration exotherm test protocol.

Sample	Water-Glue Ratio	Sample Quality	
		Cement/g	Flotation Tailings/g
S1	0.63	10	0
S2	0.63	7	3

4. Results and Discussion

4.1. Results of the One-Way Test

4.1.1. Effect of Ash on CFTFM Performance

Seven sets of flotation tailing specimens, numbered A1 to A7, were selected with ash contents of 50.1%, 52.2%, 54.5%, 58.8%, 62.8%, 66.3%, and 71%. Flotation tailings specimens were mixed with cement at a mass fraction of w = 30% to prepare the CFTFM, which was tested for uniaxial compressive strength, slump, and water secretion.

The effect of ash on the CFTFM performance is shown in Figure 3. The highest 7d and 28d uniaxial compressive strengths of the CFTFM were achieved when the ash content of the flotation tailings was 58.8%, reaching 1.7 and 2.26 MPa, respectively. The slump increased and then decreased with increasing ash content, reaching a maximum of 58.8% ash (259 mm). The results of the sample slurry water secretion rate tests are shown in Figure 2b. The water secretion rate of each sample group tended to stabilize at approximately 90 min, with the ash content increasing, the water secretion rate gradually decreasing, and the water secretion rate decreasing. The flotation tailings had a minimum water secretion rate of 9.8% at 71% ash content. Owing to the good volcanic ash activity of the flotation tailings, the incorporation promotes the hydration rate of the cement [20,21] and affects the filling slurry secretion rate; however, the effect of ash difference on the slump of the slurry is not significant.

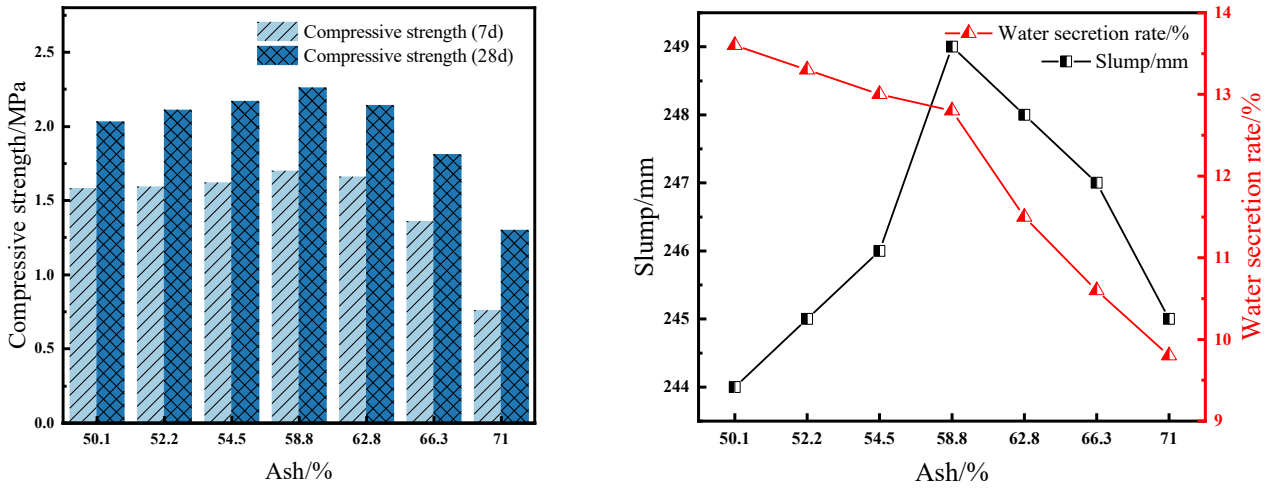

(**a**) Effect of ash on compressive strength (**b**) Effect of ash on slump and water secretion rate

Figure 3. Effect of ash on CFTFM performance.

4.1.2. Effect of Doping on the Performance of CFTFM

The CFTFM was prepared by blending the flotation tailings into the gelling material according to mass fractions of 0, 10%, 20%, 30%, 40%, 50%, and 60%, numbered B1 to B7, respectively. This was undertaken to investigate the effect of flotation tailings mixing

amount on the compressive strength, slump, and water secretion rate of the CFTFM. The effects of different doping levels on the CFTFM performance are shown in Figure 4.

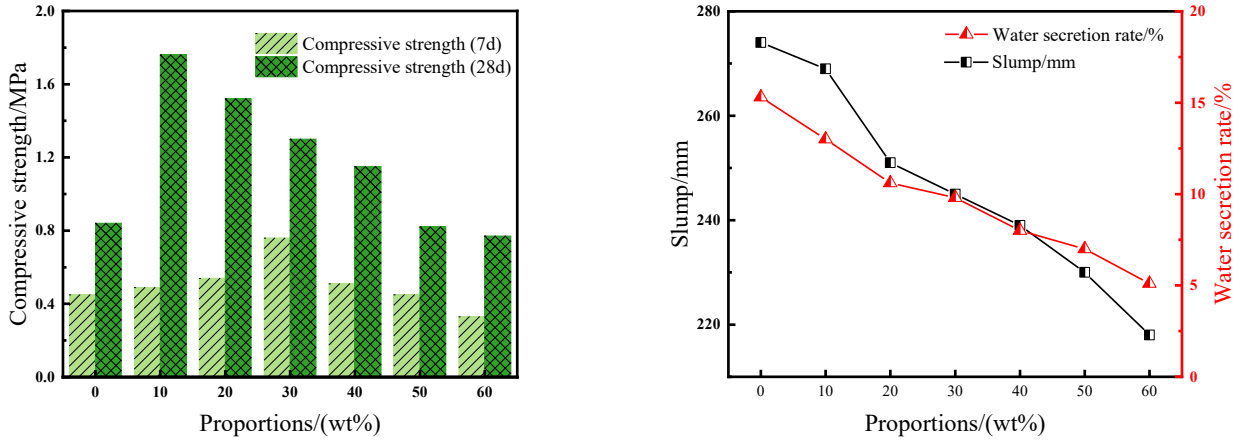

(**a**) Effect of proportions on compressive strength (**b**) Effect of proportions on slump and water secretion

Figure 4. Effect of proportions on CFTFM performance.

The 7d and 28d uniaxial compressive strengths of the CFTFM tended to increase and then decrease, owing to the increasing blending of flotation tailings. The 7d uniaxial compressive strength of the CFTFM was highest at 30%, reaching 0.76 MPa, which was higher than that of the pure cement specimen (0.45 MPa). The highest CFTFM 28d uniaxial compressive strength of 1.76 MPa was achieved at a proportion of 10%. The mechanism of the effect of the admixture on the performance of the CFTFM is that the early strength of the filler is mainly based on the hydration reaction of the cement, with the dissolution of tricalcium silicate in the cement clinker reacting with gypsum to form calcium alumina [22]. Subsequently, hydrated calcium silicate gels were formed in large quantities, releasing the heat of hydration. Coal flotation tailings have good surface properties and can adsorb large amounts of $Ca(OH)_2$. At the same time, coal flotation tailings contain a large amount of active silica and aluminum, which provide good conditions for the formation of hydrated calcium silicate gel, thus accelerating the rate of the hydration reaction. As a result, when flotation tailings are increased, the rate of hydration of the filling material is promoted, and the filling body exhibits a high early strength. The uniaxial compressive strength of the CFTFM was the lowest when the flotation tailings were blended at 60%, at which point the blending was too high and the cement content was significantly reduced, reducing the hydration capacity of the cementitious material and resulting in a poorer CFTFM performance [23].

The results of the slurry secretion rate tests for each specimen are presented in Figure 4b. The water secretion rate gradually decreased as the amount of flotation tailings increased, and the effect of the proportion on the filling slurry secretion rate was more significant. The higher the proportion, the faster the rate of water secretion, which tends to stabilize within a relatively short period. At a proportion of 60%, the slurry water secretion rate reached a minimum of 5.1%, which was much lower than the water secretion rate at a dosing level of 0 (15.3%).

The effect of the proportion of flotation tailings on the slump of the CFTFM is shown in Figure 4b. The CFTFM slump decreased with the increased blending of the flotation tailings, with the lowest slump (218 mm) at 60% proportions [24,25]. The admixture of flotation tailings is the main factor affecting the slump of the CFTFM because flotation tailings and gangue, as the main filling aggregates, determine the particle gradation composition of the filling material [26]. Good particle gradation can cause the coarse and fine particles in the slurry to be evenly mixed so that the slurry has good fluidity.

4.1.3. Effect of Calcination Temperature on the Performance of CFTFM

The volcanic ash activity of flotation tailings can be significantly increased by heat treatment, allowing the preparation of cement and concrete materials with different properties [27]. There are various methods to stimulate the activity of tailing solid waste, such as physical and chemical activation. Thermal activation is the most effective method for enhancing the volcanic ash activity of a material by destroying its crystal structure [28]. To investigate the effect of different calcination temperatures on the volcanic ash activity of flotation tailings, flotation tailings with an ash content of 71% were calcined at 650, 700, 750, 800, 850, 900, and 950 °C for 3 h. Specimens C1 to C7 were tested for uniaxial compressive strength, slump, and water retention.

The effect of the calcination temperature on the performance of the CFTFM is shown in Figure 5. The uniaxial compressive strength of the calcined CFTFM was significantly higher than that of the untreated CFTFM. As the calcination temperature increases, the uniaxial compressive strength tends to increase and then decrease, reaching a maximum value of 4.8 and 6.73 MPa at a calcination temperature of 800 °C for 7d and 28d, respectively. The overall slump tended to decrease gradually, and when the calcination temperature exceeded 800 °C, the slump of the specimen started to fall below 200 mm, which was below the minimum requirement for pipeline transport of the filling material. As shown in Figure 4b, the secretion rate tended to decrease from 650 to 950 °C, with a maximum secretion rate of 7.1% at a calcination temperature of 650 °C and a minimum of 3.9% at 950 °C.

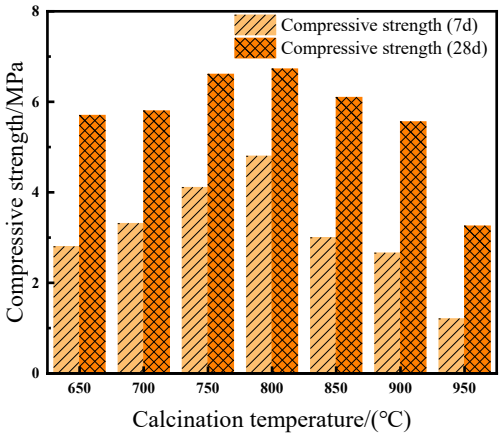

(**a**) Effect of calcination temperature on strength

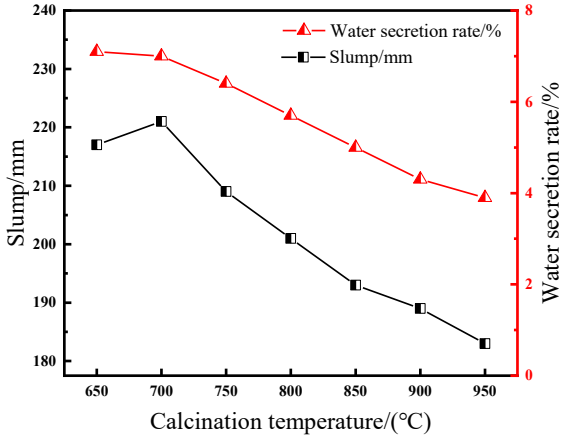

(**b**) Effect of calcination temperature on slump and water secretion rate

Figure 5. Effect of calcination temperature on CFTFM performance.

The volcanic ash activity of the flotation tailings increased substantially after calcination treatment. When the filling material is mixed with water, the components begin to dissolve and adsorb. A large amount of active material adsorbs hydration products, such as $Ca(OH)_2$ generated by hydration, providing a good spatial structure and facilitating the positive movement of the reaction [29,30]. Therefore, it exhibited high early compressive strength. However, the calcination process is expensive and the slump is significantly reduced after calcination above 800 °C, which is not conducive to practical industrial applications of the filling process. The calcination treatment temperature of the flotation tailings should not be higher than 800 °C.

4.2. Response Surface Test Results

4.2.1. Response Surface Tests

The results of the response surface tests are listed in Table 4. The 28d uniaxial compressive strength of the CFTFM varied from 0.57 to 8.0 MPa.

Table 4. Response surface test results.

Serial Number	A. Ash/%	B. Proportions/(*w*%)	C. Calcination Temperature/°C	Y. Compressive Strength/MPa
1	50.1	10	800	1.86
2	71	10	800	0.66
3	50.1	50	800	3.37
4	71	50	800	0.75
5	50.1	30	650	4.55
6	71	30	650	0.77
7	50.1	30	950	2.86
8	71	30	950	3.26
9	60.55	10	650	4.9
10	60.55	50	650	4.65
11	60.55	10	950	1.92
12	60.55	50	950	1.88
13	60.55	30	800	7.25
14	60.55	30	800	7.2
15	60.55	30	800	7.15
16	60.55	30	800	8.0
17	60.55	30	800	6.23

4.2.2. Regression Equation and Analysis of Variance

A quadratic polynomial regression equation was obtained by fitting the regression analysis to the data listed in Table 4. The regression Equation (1) is as follows:

$$Y = 7.17 - 0.9A + 0.1638B - 0.6188C - 0.355AB + 1.05AC + 0.0525BC - 2.99A^2 - 2.51B^2 - 1.31C^2 \quad (1)$$

The analysis of variance for the regression model is shown in Table 5.

Table 5. Analysis of variance for the regression model.

Source	Sum of Squares	df	Mean Square	F-Value	*p*-Value	
Model	93.58	9	10.40	9.82	0.0033	**
A-Ash	6.48	1	6.48	6.12	0.0426	*
B- Proportions	0.2145	1	0.2145	0.2025	0.6663	
C- Compressive strength	3.06	1	3.06	2.89	0.1328	
AB	0.5041	1	0.5041	0.4760	0.5125	
AC	4.37	1	4.37	4.12	0.0818	
BC	0.0110	1	0.0110	0.0104	0.9216	
A^2	37.69	1	37.69	35.58	0.0006	**
B^2	26.62	1	26.62	25.13	0.0015	**
C^2	7.27	1	7.27	6.87	0.0344	*
Residual	7.41	7	1.06			
Lack of Fit	5.83	3	1.94	4.92	0.0789	not significant
Pure Error	1.58	4	0.3950			
Cor Total	101.00	16				

Note: * indicates $p < 0.05$, significant difference; ** indicates $p < 0.01$, highly significant difference, as in the table below. The df in the table represents degrees of freedom.

As shown in Table 5, the regression model was highly significant ($F = 9.82$, $p < 0.01$), indicating that it was a good fit for the measured values. $R^2 = 0.9266$ and $R_{adj}^2 = 0.8322$ indicated that the model is a good fit for the response values, and can respond to the effects of the variables on the response values. A comparison of the model predictions with sample data is presented in Figure 6. The uniaxial compressive strength test was not sufficiently accurate because of the lack of homogeneous material mixing in the filling material test blocks and the inaccuracy of the individual data, resulting in the model-predicted values

being more divergent from the actual measured data. The effects of the primary term A and secondary terms A^2 and B^2 on the uniaxial compressive strength of the filling material are highly significant, while the primary terms B and C, interactive terms AB, AC, and BC, and the secondary term C^2 were not significant. By comparing the F-values, it can be seen that the order of magnitude of the influence of each factor on the uniaxial compressive strength of the filling material is ash (A) > calcination temperature (C) > proportions (B).

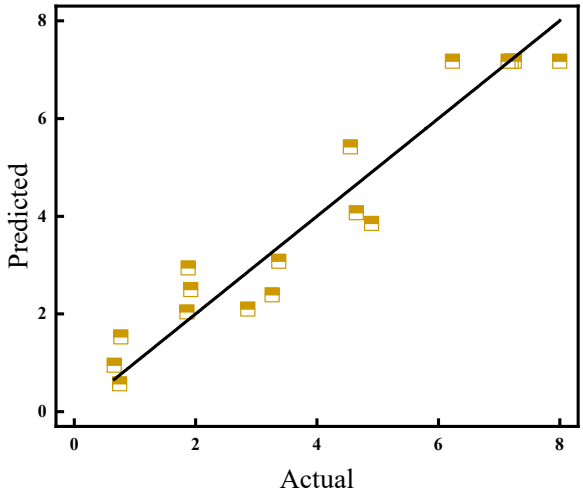

Figure 6. Comparison of predicted and measured values.

4.2.3. Response Surface Analysis

The effect of the interaction of these factors on the uniaxial compressive strength of the CFTFM is shown in Figure 7. The order of the effect of the interaction on the uniaxial compressive strength was AC > AB > BC, which is consistent with the determination of the F-value in the ANOVA.

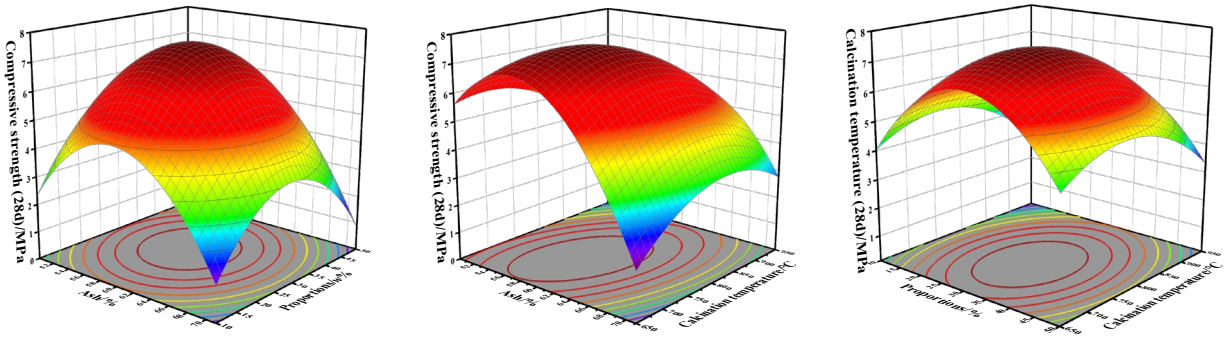

(**a**) Ash and Proportions interactions

(**b**) Ash and calcination temperature interaction

(**c**) Proportions and calcination temperature interaction

Figure 7. Effect of the interaction of factors on the compressive strength of CFTFM.

4.2.4. Optimization of the Regression Model

As the effect of insignificant terms on the regression model can interfere with the predicted values of the model and lead to overfitting, the effects of AB, AC, and BC on the response surface model were removed to reduce the complexity of the model. The optimized regression Equation (2) is as follows:

$$Y = 7.17 - 0.9A + 0.1638B - 0.6188C - 2.99A^2 - 2.51B^2 - 1.31C^2 \quad (2)$$

The equation analysis of the optimized regression model is shown in Table 6.

Table 6. Analysis of variance for the optimized regression model.

Source	Sum of Squares	df	Mean Square	F-Value	*p*-Value	
Model	88.70	6	14.78	12.02	0.0005	**
A-Ash	6.48	1	6.48	5.27	0.0446	*
B- Proportions	0.2145	1	0.2145	0.1744	0.6850	
C- calcination temperature	3.06	1	3.06	2.49	0.1456	
A^2	37.69	1	37.69	30.65	0.0002	**
B^2	26.62	1	26.62	21.65	0.0009	**
C^2	7.27	1	7.27	5.91	0.0353	*
Residual	12.30	10	1.23			
Lack of Fit	10.72	6	1.79	4.52	0.0829	not significant
Pure Error	1.58	4	0.3950			
Cor Total	101.00	16				

Note: * indicates $p < 0.05$, significant difference; ** indicates $p < 0.01$, highly significant difference, as in the table below. The df in the table represents degrees of freedom.

The ANOVA of the optimized regression model is presented in Table 6. The optimized regression model was highly significant (F = 12.02, $p = 0.0005$), and the misfit term was not significant (F = 4.52, $p > 0.05$), indicating that the optimized regression model is suitable for fitting the response values. $R^2 = 0.8782$, indicating a good fit between the regression model and the response values. The difference between $R_{pred}{}^2 = 0.5511$ and $R_{adj}{}^2 = 0.8052$ was small, indicating that the optimized model was a good predictor.

4.2.5. Confirmation and Verification of the Optimum Proportion of Flotation Tailings

The regression model analysis resulted in the optimum conditions for pre-treatment of the flotation tailings in the filling material as 58.9816% ash, 30.6454% proportions, and a calcination temperature of 764.805 °C. The predicted response value was 7.30918 MPa with a desirability of 0.906. The optimum conditions were modified in conjunction with the actual operation to 59% ash, 30% proportions, and a calcination temperature of 765 °C. After three validation tests, an average uniaxial compressive strength of 7.02 MPa was obtained for the filling material, with a relative error of 3.96% from the model prediction. This shows that the optimized regression model has a good predictive performance, and the optimized flotation tailing pre-treatment conditions are reliable and can be used for the preparation of the CFTFM.

4.3. Results of Exothermic Hydration Tests

The curves of the exothermic rate of hydration as a function of time, and the cumulative heat release during the hydration of samples S1 and S2, are shown in Figure 8. The exothermic process of hydration of cement-based materials is generally divided into five phases: rapid reaction, induction, acceleration, deceleration, and decay [31,32]. The characteristic values of the duration, exothermic rate, and heat release for each stage are shown in Table 7, based on the various characteristics of the exothermic rate of hydration at different stages of the CFTFM.

Table 7. Classification of the exothermic stages of hydration and the heat release and exothermic rate of each stage.

No.	Rapid Response Phase			Induction Phase			Accelerated Phase			Deceleration Phase		
	t/h	*Q*/ (J·g^{-1})	*R*/ (J·(g·h)$^{-1}$)	*t*/h	*Q*/ (J·g^{-1})	*R*/ (J·(g·h)$^{-1}$)	*t*/h	*Q*/ (J·g^{-1})	*R*/ (J·(g·h)$^{-1}$)	*t*/h	*Q*/ (J·g^{-1})	*R*/ (J·(g·h)$^{-1}$)
S1	2.2	21.9	9.89	4.5	4.3	0.94	10.1	22.4	2.21	3.4	18.1	5.32
S2	2.5	22.5	8.95	4.2	4.6	1.09	2.3	4.4	1.76	3.6	6.5	1.81

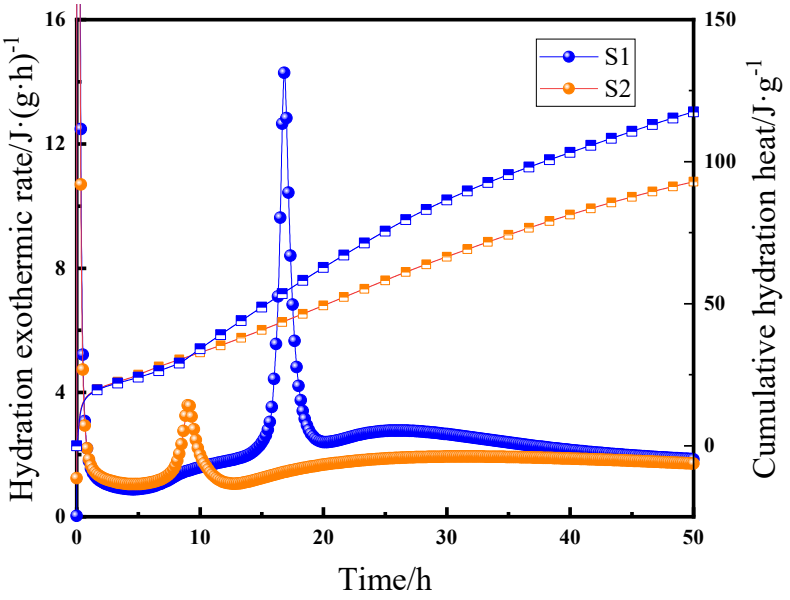

Figure 8. Rate of exothermic hydration and cumulative heat release.

As can be seen from the above diagram, the CFTFM specimens had exothermic hydration characteristics similar to those of cementitious materials. Comparing the two sets of specimens, specimen S2 had a longer rapid exothermic phase and a higher phase heat release. The duration of specimen S2 in the induction and acceleration phases was significantly shorter, and both the phase heat release and rate of heat release in the acceleration phase were significantly reduced. Compared to pure cement sample S1, the second exothermic peak of sample S2 was significantly lower and shifted forward. It can be seen that the influence of the flotation tailings on the exothermic hydration of the CFTFM is mainly concentrated in the rapid reaction phase and the induction phase. The flotation tailings have good volcanic ash activity, which reduces the exothermic heat in the acceleration phase and accelerates the exothermic rate of hydration. The reduction in cement blending owing to the incorporation of flotation tailings, and the promotion of reactive Si and Al in the flotation tailings accelerates the hydration of the cement, leading to a change in the second exothermic peak.

After the exothermic hydration curve reached the second exothermic peak, the hydration reaction entered a deceleration phase, and the exothermic rate of hydration decreased with time. The deceleration phase of specimen S2 required less time and was slower. After the deceleration phase, the hydration reaction rate gradually tends to zero and enters the decay phase, when the hydration reaction tends to stabilize.

4.4. Hydration Products and Hydration Mechanisms

4.4.1. XRD Analysis of Hydration Products

XRD analysis of hydration products was conducted at different stages of the CFTFM. The specimens were mixed well with water and placed in plastic molds for 48 h, followed by the addition of anhydrous ethanol to terminate hydration, drying in an oven, and subsequent analysis by XRD. The results of this analysis are shown in Figure 9. The hydration products generated by the filling material after 48 h of maintenance were mainly hydrated calcium silicate, calcium carbonate, and complex polymers formed from elements such as Si, Al, and Ca. The types of hydration products generated at different stages are similar but show different peak heights, with the crystalline phase content of the hydration products gradually increasing with time.

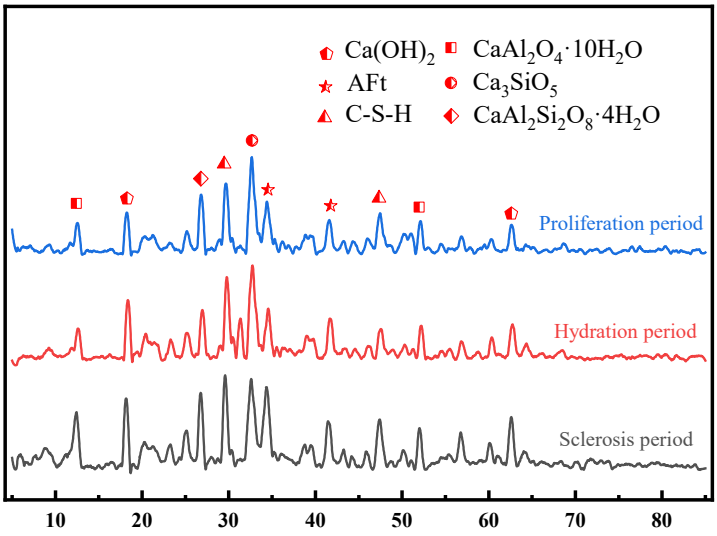

Figure 9. XRD pattern of hydration products.

4.4.2. FT-IR Analysis of Hydration Products

The hydration products of the samples at each stage of hydration were analyzed by FT-IR using a Fourier Transform Infrared Spectrometer (FT-IR Spectrometer). The infrared absorption spectra of the samples are shown in Figure 9.

The FT-IR profile of the CFTFM is shown in Figure 10. The FT-IR spectrum of the CFTFM is more complex, with absorption peaks in the range of 500–1500 cm^{-1}, and the main hydration products are silicone polymers in the form of $(SiO_3)^{3-}$ and $(SiO_4)^{4-}$ [33]. Analysis of the hydration product characteristics at different stages of hydration in the CFTFM showed that the hydration product types in the system remained unchanged, but the absorption wave numbers of components such as $(SiO_3)^{3-}$ and $(SiO_4)^{4-}$ gradually moved from low to high, and the peak shape narrowed, indicating that the degree of polymerization of the generated hydration products increased [34]. As the hydration reaction proceeded, the strength of the filling material increased, and a water-hardened substance was formed.

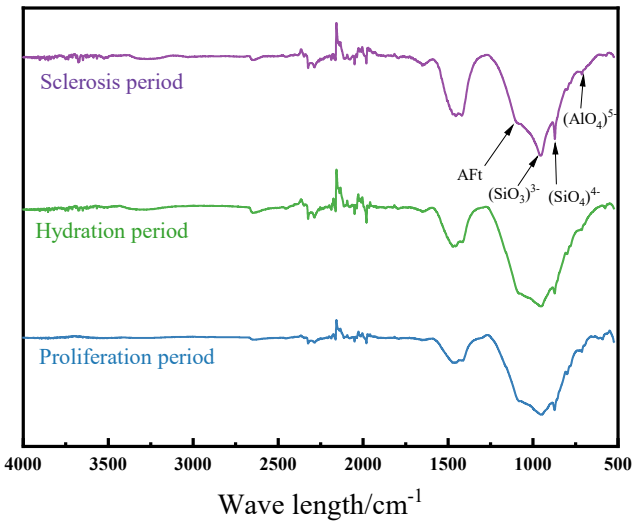

Figure 10. FT-IR spectrum of CFTFM.

4.4.3. Characterization of the Morphology of the Hydration Products

The microscopic morphology of the hydration products of the samples was photographed using a TESCAN MIRA LMS scanning electron microscope at × magnification

of 20,000. The microscopic morphologies of the hydration products at different stages of the CFTFM hydration are shown in Figure 11.

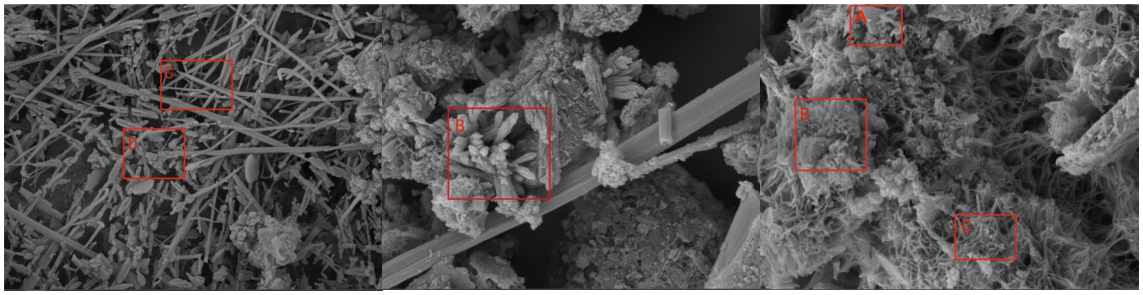

(**a**) Proliferation period (**b**) Hydration period (**c**) Sclerosis period

Figure 11. Shape of CFTFM hydration products.

The CFTFM is a complex nonhomogeneous three-phase system that undergoes a series of physical and chemical changes when mixed homogeneously with water, producing hydration products of different shapes [35]. Shown in Figure 11, A, B, C, and D are calcium hydroxide (CH), calcium hydrogenated silicate (C-S-H), calcium tri-sulfate aluminosilicate (AFt), and unreacted material, respectively. The following model was developed to describe the hydration mechanism of the CFTFM by dividing the hydration process into three stages:

Proliferation phase: as shown in Figure 11a, the components of the CFTFM dissolve rapidly after stirring with water, releasing a large number of anions and cations into the water while being exothermic, which corresponds to the first exothermic peak of the hydration exothermic curve. The first hydration product that formed after the start of hydration was AFt. The rate of hydration of the cement clinker (C_3A) slows owing to a large amount of AFt formation, resulting in the system entering the induction period. During the induction period, the hydration reaction stabilized and the resulting spike-like calcium alumina was interwoven with the unreacted tailing admixture [36]. The main chemical reactions that occur during this phase are:

$$C_3A + CH + 12H = C_4AH_{13} \quad (3)$$

$$C_4AH_{13} + 3CS'H + 14H = AFt + CH \quad (4)$$

Hydration phase: as hydration enters an accelerated phase, C_3S hydrates rapidly, forming C-S-H and CH, corresponding to the appearance of a second exothermic peak. As shown in Figure 11b, a large number of active oxides such as SiO_2 and Al_2O_3 in the flotation tailings adsorb large amounts of $Ca(OH)_2$, which accelerates the hydration reaction process [37], and promotes the hydration of the cement clinker to produce flaky CH that adheres heavily to the surface of unreacted particles. The resulting C-S-H form is not fixed, and is the main cementing material used for hardening cement. The main chemical reaction occurring within this phase is:

$$3Ca{\cdot}SiO_2 + nH_2O \rightarrow xCaO{\cdot}SiO_2{\cdot}yH_2O + (3 - x)Ca(OH)_2 \quad (5)$$

Hardening phase: the rate of exothermic formation and the phase of the architecture are low and stable. The formation of fragmented hydration products wrapped around the surface of the particles is shown in Figure 11c [38]. As the hydration products continue to increase, the particle spacing is sharply compressed, and particles of different sizes coalesce with each other under interactive forces such as van der Waals and chemical bonding forces [39]. This results in irregular hydration products such as caliche interweaving with each other, forming a reticulated structure [40]. The exothermic hydration of the filling material tends to zero, the hydration products extend towards the interior of the cohesion, and the CFTFM continuously strengthens.

5. Conclusions

(1) The order of influence of each factor of the flotation tailings on the uniaxial compressive strength of the CFTFM was ash > calcination temperature > proportions. The order of influence of the interaction on the uniaxial compressive strength was ash and calcination temperature interaction > ash and proportions interaction > proportions and calcination temperature interaction.

(2) The optimum pre-treatment conditions for the optimized flotation tailings were 59% ash, 30% proportions, and a calcination temperature of 765 °C. The optimum uniaxial compressive strength of the CFTFM was 7.02 MPa.

(3) The effect of flotation tailings on the exothermic hydration of the CFTFM was mainly on the induction and acceleration phases. With the incorporation of flotation tailings, the duration of the induction and acceleration phases reduced, the second exothermic peak occurred earlier, and the peak reduced. This decrease is due to a reduction in cement blending, and the forward shift is due to the volcanic ash active material in the tailings promoting cement hydration [37].

(4) The early hydration products of the CFTFM were calcium hydroxide, hydrated calcium silicate, and calcium alumina [39], with increasing degrees of polymerization with hydration time. A descriptive model of the hydration mechanism of the CFTFM was constructed by dividing the hydration mechanism into diffusion, hydration, and hardening phases [33].

Author Contributions: Conceptualization, D.L. and Y.F.; methodology, X.M.; validation, P.L.; formal analysis, D.L.; resources, X.D.; writing—original draft preparation, D.L.; writing—review and editing, Y.F.; visualization, D.L.; supervision, X.D. All authors have read and agreed to the published version of the manuscript.

Funding: This research is funded by the Fund for International Cooperation and Exchange of the National Natural Science Foundation of China (Grant No. 51820105006), and Key R&D Projects in Shanxi Province (Item No.: 2022ZDYF049).

Data Availability Statement: Not applicable.

Conflicts of Interest: The authors declare no conflict of interest.

References

1. Liu, J.G.; Li, X.W.; He, T. Application status and prospect of backfill mining in Chinese coal mines. *J. China Coal Soc.* **2020**, *45*, 141–150.
2. Zhang, J.X.; Mou, X.X.; Guo, G.L. Development Status of Backfilling Technology Using Raw Waste in Coal Mining. *J. Min. Saf. Eng.* **2009**, *26*, 395–401. [CrossRef]
3. Cao, H.; Gao, Q.; Zhang, X.; Guo, B. Research Progress and Development Direction of Filling Cementing Materials for Filling Mining in Iron Mines of China. *Gels* **2022**, *8*, 192. [CrossRef]
4. Feng, G.R.; Jia, X.Q.; Guo, Y.X.; Qi, T.Y.; Li, Z.; Li, J.Z.; Kang, L.X.; Liu, G.Y.; Song, K.G. Study on mixture ratio of gangue-waste concrete cemented paste backfill. *J. Min. Saf. Eng.* **2016**, *33*, 1072–1079. [CrossRef]
5. Li, J.; Li, S.; Peng, L.; Chen, B. A new method to rapidly evaluate the activity of volcanic ash materials. *Cem. Concr. Compos.* **2023**, *135*, 104833. [CrossRef]
6. Guo, Y.; Yan, K.; Cui, L.; Cheng, F. Improved extraction of alumina from coal gangue by surface mechanically grinding modification. *Powder Technol.* **2016**, *302*, 33–41. [CrossRef]
7. Moghadam, M.J.; Ajalloeian, R.; Hajiannia, A. Preparation and application of alkali-activated materials based on waste glass and coal gangue: A review. *Constr. Build Mater.* **2019**, *221*, 84–98. [CrossRef]
8. Li, Y.; Yao, Y.; Liu, X.; Sun, H.; Ni, W. Improvement on pozzolanic reactivity of coal gangue by integrated thermal and chemical activation. *Fuel* **2013**, *109*, 527–533. [CrossRef]
9. Guan, X.; Chen, J.; Zhu, M.; Gao, J. Performance of microwave-activated coal gangue powder as auxiliary cementitious material. *J. Mater. Res. Technol.* **2021**, *14*, 2799–2811. [CrossRef]
10. Kasap, T.; Yilmaz, E.; Sari, M. Effects of mineral additives and age on microstructure evolution and durability properties of sand-reinforced cementitious mine backfills. *Constr. Build Mater.* **2022**, *352*, 129079. [CrossRef]
11. Jin, J.; Qin, Z.; Lü, X.; Liu, T.; Zhang, G.; Shi, J.; Zuo, S.; Li, D. Rheology control of self-consolidating cement-tailings grout for the feasible use in coal gangue-filled backfill. *Constr. Build Mater.* **2022**, *316*, 125836. [CrossRef]

12. Hou, Y.Q.; Yin, S.H.; Dai, C.Q.; Cao, Y. Rheological properties and pipeline resistance calculation model in tailings paste. *Chin. J. Nonferrous Met.* **2021**, *31*, 510–519. [CrossRef]
13. Yin, B.; Kang, T.H.; Kang, J.T.; Chen, Y.J.; Wu, L.L. The research of the hydration kinetics process and hydration mechanismof fly ash paste filling materials. *Chin. J. Rock Mech. Eng.* **2018**, *37*, 4384–4394. [CrossRef]
14. Meng, T.; Hong, Y.; Wei, H.; Xu, Q. Effect of nano-SiO_2 with different particle size on the hydration kinetics of cement. *Thermochim. Acta* **2019**, *675*, 127–133. [CrossRef]
15. Li, L.; Chen, M.; Guo, X.; Lu, L.; Wang, S.; Cheng, X.; Wang, K. Early-age hydration characteristics and kinetics of Portland cement pastes with super low w/c ratios using ice particles as mixing water. *J. Mater. Res. Technol.* **2020**, *9*, 8407–8428. [CrossRef]
16. *GB/T 50080-2016*; Standard for Test Method of Performance on Ordinary Fresh Concrete. Standards Press of China: Beijing, China, 2016; p. 99.
17. *GB/T 1346-2011*; Test Methods for Water Requirement of Normal Consistency, Setting Time and Soundness of the Portland Cement. Standards Press of China: Beijing, China, 2011; p. 12.
18. *GB/T 50081-2019*; Standard for test methods of concrete physical and mechanical properties. China Architecture & Building Press: Beijing, China, 2003; p. 36.
19. *GB/T 23561.13-2010*; Methods for Determining the Physical and Mechanical Properties of Coal and Rock—Part 13: Methods for Determining Point Load Strength Index of Coal and Rock. Standards Press of China: Beijing, China, 2010; p. 9.
20. Wu, L.L.; Kang, T.H.; Yin, B.; Du, M.Z. Microcalorimetric test and analysis of hydration heat of fly ash paste-filling material. *J. China Coal Soc.* **2015**, *40*, 2801–2806. [CrossRef]
21. Liu, Y.; Lei, S.; Lin, M.; Li, Y.; Ye, Z.; Fan, Y. Assessment of pozzolanic activity of calcined coal-series kaolin. *Appl. Clay Sci.* **2017**, *143*, 159–167. [CrossRef]
22. Liu, X.; Feng, P.; Shen, X.Y.; Wang, H.C.; Zhao, L.X.; Mu, S.; Ran, Q.P.; Mou, C.W. Advances in the Understanding of Cement Hydrate—Calcium Silicate Hydrate (C-S-H). *Mater. Rep.* **2021**, *35*, 9157–9167. [CrossRef]
23. Shuang-xi, Z. Study on the reaction degree of calcined coal gangue powder in blended cement by selective solution method. *Procedia Earth Planet. Sci.* **2009**, *1*, 634–639. [CrossRef]
24. Zhang, J.Q.; Yang, K.; He, X.; Wei, Z.; Zhao, X.Y.; Fang, J.J. Experimental Study on Strength Development and Engineering Performance of Coal-Based Solid Waste Paste Filling Material. *Metals* **2022**, *12*, 1155. [CrossRef]
25. Zhang, X.G.; Lin, J.; Liu, J.X.; Li, F.; Pang, Z.Z. Investigation of Hydraulic-Mechanical Properties of Paste Backfill Containing Coal Gangue-Fly Ash and Its Application in an Underground Coal Mine. *Energies* **2017**, *10*, 1309. [CrossRef]
26. Ulusoy, U. A Review of Particle Shape Effects on Material Properties for Various Engineering Applications: From Macro to Nanoscale. *Minerals* **2023**, *13*, 91. [CrossRef]
27. Cheng, H.L.; Yang, F.H.; Ma, B.G.; Zhang, J.; Hao, L.W.; Liu, G.Q. Composite Activation of High Alumina Coal Gangue and Analysis on Its Pozzolanic Effect. *J. Build. Mater.* **2016**, *19*, 248–254. [CrossRef]
28. Zhang, J.X.; Sun, H.H.; Wan, J.H.; Zhang, N. Analysis of pozzolanic activity evaluation methods for calcined coal gangue. *J. Harbin Inst. Technol.* **2010**, *42*, 1438–1443. [CrossRef]
29. Su, Z.; Li, X.; Zhang, Q. Influence of thermally activated coal gangue powder on the structure of the interfacial transition zone in concrete. *J. Clean Prod.* **2022**, *363*, 132408. [CrossRef]
30. Hao, R.; Li, X.; Xu, P.; Liu, Q. Thermal activation and structural transformation mechanism of kaolinitic coal gangue from Jungar coalfield, Inner Mongolia, China. *Appl. Clay Sci.* **2022**, *223*, 106508. [CrossRef]
31. Luo, P.X.; Deng, N.D.; Jie, G.; Xing, C.C.; Li, Y.X. Hydration mechanism and kinetic characteristics of Ca Cl2 activated fly ash. *Environ. Eng.* **2022**, 1–11. Available online: https://kns.cnki.net/kcms/detail/11.2097.x.20221123.1629.010.html (accessed on 1 January 2023).
32. Yin, B.; Kang, T.; Kang, J.; Chen, Y.; Wu, L.; Du, M. Investigation of the hydration kinetics and microstructure formation mechanism of fresh fly ash cemented filling materials based on hydration heat and volume resistivity characteristics. *Appl. Clay Sci.* **2018**, *166*, 146–158. [CrossRef]
33. Xiao, J.M.; Li, H.; Zhu, H.M.; Dang, Y. Analysis on Hydration Products of Cement-slag Complex Binder Pastes by FTIR and NMR. *J. Mater. Sci. Eng.* **2018**, *36*, 644–649. [CrossRef]
34. Gao, B.; Poduska, K.M. Tracking Amorphous Calcium Carbonate Crystallization Products with Far-Infrared Spectroscopy. *Minerals* **2023**, *13*, 110. [CrossRef]
35. Ji, X.; Gu, X.; Wang, Z.; Xu, S.; Jiang, H.; Yilmaz, E. Admixture Effects on the Rheological/Mechanical Behavior and Micro-Structure Evolution of Alkali-Activated Slag Backfills. *Minerals* **2023**, *13*, 30. [CrossRef]
36. Feng, Y.; Li, F.; Qi, W.; Ren, Q.; Qi, W.; Duan, G.; Zheng, K.; Han, Y.; Pang, H. Mechanical Properties and Microstructure of Iron Tailings Cemented Paste Backfills Using Carbide Slag-Activated Ground Granulated Blast-Furnace Slag as Alternative Binder. *Minerals* **2022**, *12*, 1549. [CrossRef]
37. Sun, Q.; Tian, S.; Sun, Q.; Li, B.; Cai, C.; Xia, Y.; Wei, X.; Mu, Q. Preparation and microstructure of fly ash geopolymer paste backfill material. *J. Clean Prod.* **2019**, *225*, 376–390. [CrossRef]
38. Zhu, Z.Y.; Wang, Z.P.; Zhou, Y.; Chen, Y.T.; Wu, K. In-situ Study on Micro-Nano Structure of Portland Cement Hydration Products. *J. Chin. Ceram. Soc.* **2021**, *49*, 1699–1705. [CrossRef]

39. Zhang, W.S.; Xu, J.H.; Liu, L.; Ye, J.Y.; Qian, J.S. Effect of Liquid Environment on Hydration Activity of Ternesite–Dicalcium Silicate Composite Minerals. *J. Chin. Ceram. Soc.* **2022**, *50*, 2070–2077. [CrossRef]
40. Yang, J.J.; Lan, M.Z.; Wang, J.F.; Pei, T.R.; Ni, Y.L. Research on hydration properties of multiple solid waste-based cementitious materials. *New Build. Mater.* **2022**, *49*, 107–113. [CrossRef]